Annals of Biomedical Engineering, Vol. 43, No. 12, December 2015 *(© 2015)* pp. 2838–2851
DOI: 10.1007/s10439-015-1357-9

Modeling of Experimental Atherosclerotic Plaque Delamination

XIAOCHANG LENG,[1] XIN CHEN,[1] XIAOMIN DENG,[1] MICHAEL A. SUTTON,[1] and SUSAN M. LESSNER[2]

[1]Department of Mechanical Engineering, University of South Carolina, Columbia, SC 29208, USA; and [2]Department of Cell Biology & Anatomy, University of South Carolina, Columbia, SC 29208, USA

(Received 6 February 2015; accepted 8 June 2015; published online 23 June 2015)

Associate Editor Scott I Simon oversaw the review of this article.

Abstract—A cohesive zone model (CZM) approach is applied to simulate atherosclerotic plaque delamination experiments in mouse abdominal aorta specimens. A three-dimensional finite element model is developed for the experiments. The aortic wall is treated as a fiber-reinforced, highly deformable, incompressible material, and the Holzapfel–Gasser–Ogden (HGO) model is adopted for the aortic bulk material behavior. Cohesive elements are placed along the plaque-media interface along which delamination occurs. The 3D specimen geometry is created based on images from the experiments and certain simplifying approximations. A set of HGO and CZM parameter values is determined based on values suggested in the literature and through matching simulation predictions of the load vs. load-point displacement curve with experimental measurements for one loading–delamination–unloading cycle. Using this set of parameter values, simulation predictions for four other loading–delamination–unloading cycles are obtained, which show good agreement with experimental measurements. The findings of the current study demonstrate the applicability of the CZM approach in arterial tissue failure simulations.

Keywords—Plaque, Delamination, Aorta, Atherosclerosis, Finite element, Cohesive zone, Energy release rate.

INTRODUCTION

Atherosclerotic plaque rupture often happens suddenly and unpredictably *in vivo*, causing roughly 75% of all newly developed and recurring myocardial infarctions and affecting approximately 1.1 million people in the USA per year with a 40% fatality rate.[31]

A common plaque rupture site is the shoulder region where the interface between the plaque and the underlying vascular wall is located.[22] This site is prone to delaminate along the plaque-media interface, for example, when the arterial wall experiences large expansion under balloon angioplasty.[3] In general, due to mismatch in mechanical properties across a vessel wall interface, interlayer shear stress concentration is expected to occur at geometric discontinuities (e.g., along the edge of the plaque-media interface) when the artery is deformed, which may cause initiation of interfacial delamination. Plaque delamination (dissection) at the shoulder with intimal flap formation during balloon angioplasty and stenting has been demonstrated by *in vivo* imaging modalities such as intravascular ultrasound and optical coherence tomography.[12,20,25,27] Shear loading due to flow induced shear traction on the plaque surface is also expected to contribute to the initial tearing and delamination of the plaque. The subsequent delamination growth may be mixed-mode, in which the Mode I (opening mode) component can be significant. The Mode I component can be due to the normal loading from flow pressure (e.g., immediately after the initial tear and delamination) and/or due to a peeling action created by the flow-induced shear traction on the now delaminated portion of the plaque. Once delamination occurs, it seems that this shear traction will tend to pull the delaminated plaque in the direction of the flow, because the plaque is compliant and the delaminated portion will tend to bend in the flow direction. As such, it is important to understand plaque delamination (dissection) failure in order to develop effective approaches for treatment and intervention.

Atherosclerotic plaque delamination depends both on the deformation and stress experienced by the arterial wall and on the interfacial strength between the plaque and the vascular wall. One measure of the interfacial strength is the critical energy release rate, which is the energy required to delaminate a unit area of the plaque from the underlying vascular wall. This critical energy release rate can be measured in plaque delamination experiments and can serve as an input to

Address correspondence to Xiaomin Deng, Department of Mechanical Engineering, University of South Carolina, Columbia, SC 29208, USA. Electronic mail: deng@cec.sc.edu

a mechanics model (such as the cohesive zone model) that describes the interfacial strength mathematically.

In the current study, a finite element modeling and simulation approach for atherosclerotic plaque delamination experiments has been developed. In particular, plaque delamination experiments performed on apolipoprotein E-knockout (ApoE-KO) mouse aorta specimens are modeled in order to gain an understanding of the role of mechanical failure in human atherosclerosis because the ApoE-KO mouse aorta has been shown to develop atherosclerotic lesions similar in many respects to those seen in humans.[23] It is noted that the modeling approach developed in this study can deal with mixed-mode delamination failure. The particular delamination experiments noted above, in which a Mode I type delamination occurs due to the peeling of the delaminated portion of the plaque from the aorta wall, are used to demonstrate and validate this approach because of their availability and the lack of other types of experimental data in the literature. This study tries to establish the credibility and viability of this approach in order to provide a strong basis for its application to other clinically relevant failure modes such as those involving shear failure.

The cohesive zone model (CZM) approach is employed in this study to model the delamination behavior at the plaque-media interface. It is noted that the CZM is a general approach for modeling separation processes in solid materials, including debonding and delamination along interfaces. In particular, CZM has been proven to be an effective way of modeling delamination failure in composite materials.[28] Atherosclerotic plaque delamination at the plaque shoulder site is analogous to the common delamination damage phenomenon between layers in laminated composites, and thus the CZM seems applicable, although to the authors' knowledge, it has not been applied in the literature to the study of experimental plaque delamination. While the CZM has been widely used in studies of fracture failures in engineering materials, the use of CZM in studies of failure in arterial materials has been very limited. These limited studies include analysis of fissuring and dissection in the human plaque during balloon angioplasty intervention,[15] modeling the propagation of dissection of human aortic media,[14] and simulation of arterial dissection under pressure.[13]

In the current study, the atherosclerotic plaque delamination phenomenon is investigated through modeling and simulation of experiments performed on ApoE-KO mouse aorta specimens in which a plaque is peeled off from an arterial wall. A three-dimensional (3D) finite element model for the experiments is developed, in which the Holzapfel–Gasser–Ogden (HGO) model[16,19] for the bulk arterial material behavior and a CZM for the plaque-media interface behavior are adopted. Simulation predictions of the load vs. load-point displacement curve are compared with experimental measurements as validation for the proposed modeling approach. Also, uncertainties about the specimen geometry are analyzed in order to understand how these factors affect the predicted load vs. load-point displacement responses.

MATERIAL MODEL

Arteries are usually modeled as nearly incompressible and highly deformable composite materials that exhibit a nonlinear stress–strain response with typical stiffening at the physiological strain level.[13] To simulate atherosclerotic plaque delamination in mouse aorta, we adopt the HGO model[16,19] for the bulk material behavior and the CZM[5] for the delamination behavior along the plaque-media interface. In the HGO model, the bulk material of each artery layer is treated as a fiber-reinforced material with fibers symmetrically distributed in regard to the axial direction of the aorta. In the CZM, a triangular shaped traction–separation law is implemented to govern the delamination procedure.

Bulk Material for the Mouse Aorta

The HGO model assumes that collagen fibers are oriented parallel to the arterial wall,[16] thus neglecting the out-of-plane orientation component useful in preventing out-of-plane shearing.[18] The strain energy function in the HGO model is given by[16]

$$\overline{\psi} = \frac{\mu}{2}\left(\overline{I}_1 - 3\right) + \frac{k_1}{2k_2}\left[e^{k_2\left[\kappa\overline{I}_1 + (1-3\kappa)\overline{I}_{41} - 1\right]^2} - 1\right] + \frac{k_1}{2k_2}\left[e^{k_2\left[\kappa\overline{I}_1 + (1-3\kappa)\overline{I}_{42} - 1\right]^2} - 1\right] \tag{1}$$

In the above expression, μ is the neo-Hookean parameter, which characterizes the shear modulus of the solid without fibers; k_1 is a parameter related to the relative stiffness of the two families of fibers in the small strain range; k_2 is a dimensionless stiffness parameter for the large strain range; and κ ($0 \le \kappa \le 1/3$) is the dispersion parameter that characterizes the dispersion of the two families of fibers along the two mean distributed directions. Also in Eq. (1), $\overline{I}_1 = \mathrm{tr}(\overline{\boldsymbol{C}})$ denotes the first invariant of $\overline{\boldsymbol{C}}$, which is a modified counterpart of the right Cauchy-Green strain tensor $\boldsymbol{C}$ and is given by $\overline{\boldsymbol{C}} = \overline{\boldsymbol{F}}^T\overline{\boldsymbol{F}}$; $\overline{\boldsymbol{F}} = J^{-1/3}\boldsymbol{F}$, where $\boldsymbol{F}$ is the deformation gradient and $J = \det(\boldsymbol{F})$; and

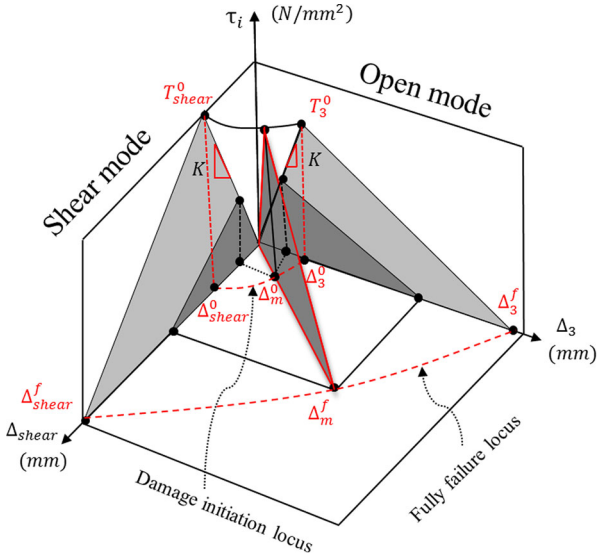

FIGURE 1. Interfacial triangular mixed-mode cohesive traction–separation law.

$\bar{I}_{41} = \boldsymbol{a}_{01} \cdot \bar{\boldsymbol{C}}\boldsymbol{a}_{01}$ and $\bar{I}_{42} = \boldsymbol{a}_{02} \cdot \bar{\boldsymbol{C}}\boldsymbol{a}_{02}$ are tensor invariants equal to the square of the stretch in the direction of, respectively, $\boldsymbol{a}_{01}$ and $\boldsymbol{a}_{02}$, which are vectors representing the directions of the two families of fibers (with β as the angle between one family of fibers and the axial direction).

Cohesive Zone Model

The CZM is implemented in the current study through a user UEL subroutine in ABAQUS.[2] It describes the relationship between the cohesive tractions between the two faces of an interface and the separations (displacement jumps) across the interface. Figure 1 shows an illustration of the mixed-mode traction–separation law, which gives the opening-mode version when projected onto the back surface of the box and the shear-mode version when projected onto the left surface of the box. The triangles in the opening-mode and shear mode coordinate planes represent the traction response as a function of separation under pure normal and pure shear deformation conditions. The triangle on a plane between these two planes represents the traction–separation relationship for a mixed-mode case. According to the CZM, the delamination failure of the plaque-media interface involves three steps. The first step is damage initiation, which refers to the start of degradation of the cohesive element when an effective displacement jump Δ^0_m is reached (as shown on the damage initiation locus in Fig. 1). At the instant of damage initiation, the traction reaches the maximum value at the peak point of the triangle. The second step is damage evolution, during which damage accumulation occurs in the cohesive element. The third step is complete failure of the cohesive element after the effective displacement jump reaches a critical effective separation value Δ^f_m (as shown on the full failure locus in Fig. 1).[28]

The failure criterion proposed by Benzeggagh and Kenane[4] has been found to fit experimental results accurately and is employed in the current study to govern the failure of the cohesive element. Based on this criterion, the mixed-mode fracture toughness (the critical energy release rate) is expressed as:

$$G_c = G_{Ic} + (G_{IIc} - G_{Ic})\left(\frac{G_{shear}}{G_T}\right)^{\alpha} \tag{2}$$

where G_{Ic}, G_{IIc} are the fracture toughness values of the material for mode I (the opening mode) and mode II (the in-plane shear mode), respectively. The total energy release rate and the energy release rate for shear loading in Eq. (2) is defined by

$$G_T = G_I + G_{II} + G_{III} \tag{3}$$

$$G_{shear} = G_{II} + G_{III} \tag{4}$$

where G_I, G_{II} and G_{III} represent the mode I, mode II and mode III (the out-of-plane shear mode) energy release rate, respectively. The cohesive law that governs material separation process can be written as:

$$\tau_i = \tau(\Delta_i) \tag{5}$$

$$\Delta^0_3 = T^0_3/K \tag{6}$$

$$\Delta^0_{shear} = T^0_{shear}/K \tag{7}$$

where τ_i $(i = 1, 2, 3)$ are the effective cohesive tractions, which are functions of the effective displacement jumps Δ_i in the local coordinates; Δ^0_3 and Δ^0_{shear} are the displacement jumps corresponding to damage initiation under pure Mode I and Mode II conditions, respectively; and T^0_3 and T^0_{shear} are the strengths of the cohesive interface along the normal direction and tangential direction, respectively. Details of the cohesive finite element can be found in Ref. 28.

EXPERIMENTAL PROCESS

The current study is focused on the modeling of atherosclerotic plaque delamination experiments performed on mouse aorta specimens reported in Ref. 32. In these experiments, ApoE-KO mice were fed a high-fat (42% of total calories) Western-style diet for 8 months, starting at the age of 6 weeks, in order to develop atherosclerosis throughout the aorta.[24] At the start of the experiment, a small initial delamination was carefully introduced by a scalpel at the proximal end of the

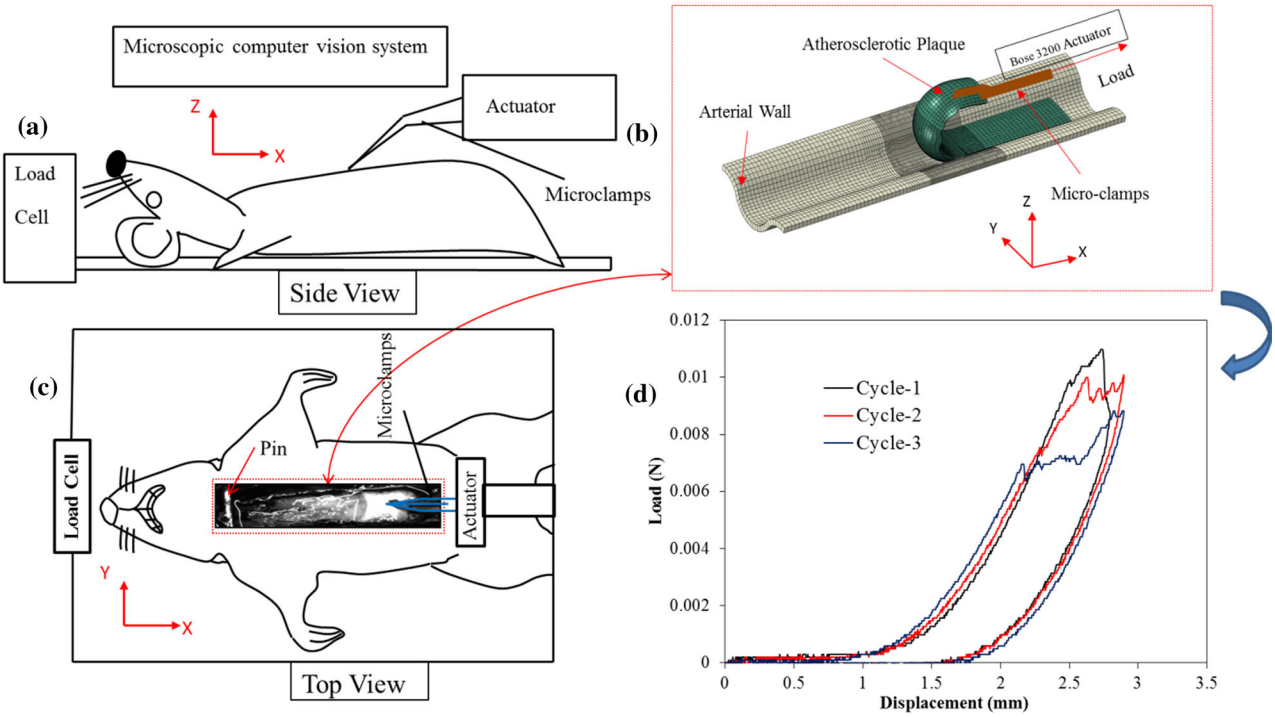

FIGURE 2. A schematic of the atherosclerotic plaque delamination experimental setup: (a) side view of the schematic diagram of the experiment, a mouse specimen on a loading table; (b) a schematic diagram of the experimental process represented by a finite element model; (c) top view of the schematic diagram of the experiment; (d) three typical consecutive experimental load vs. load-point displacement curves.

plaque, so that the micro-clamp can clamp the plaque edge, as shown in Fig. 2. The plaque was delaminated *in situ*. Pins were placed at both ends of a specimen to prevent excessive outward motion of the aorta, as shown in Figs. 2c and 3. The tissues surrounding and underlying the aorta provide considerable structural support and restrict the outward motion of the aorta during the delamination procedure; in particular, the dorsally-oriented intercostal branches prevent the outward motion of the thoracic aorta.[32]

A mouse carcass with exposed aorta was fastened to a small plate connected to the load cell of a Bose ELF 3200 for load data recording. The small delamination on the proximal end of the plaque was gripped by a pair of micro-clamps connected to the Bose ELF 3200 actuator, which applies sequential loading–delamination–unloading cycles, as shown in Fig. 2d. The delamination process was recorded by a computer vision system which was placed a certain distance above the mouse carcass, and one of the recorded images is shown in the center insert box in Fig. 2c. For each experiment, a load–displacement curve with multiple loading–delamination–unloading cycles was obtained, and three sequential loading–unloading cycles from specimen #1 are shown in Fig. 2d. After the experiment, the specimens were prepared for histological analyses, which reveal that the plaque delamination took place between the plaque and the underlying internal elastic lamina (IEL), instead of within the media.[32]

NUMERICAL SIMULATIONS OF ATHEROSCLEROTIC PLAQUE DELAMINATION

Simulation Model

An important part of the plaque delamination simulation model is the geometric dimensions of the aorta (e.g., diameter, thickness of wall, length and curvature) and plaque (e.g., thickness and length of plaque along the longitudinal direction of aorta) since errors in the geometric dimensions will lead to errors in simulation predictions. Since limited geometric values were obtained from the delamination experiments being modeled in this study, several considerations and assumptions are found necessary to create the simulation model (the finite element model).

First, the digitized images from the plaque delamination experiments are used to measure certain geometry data directly, including the length and width of the plaque. Second, reference geometry data from the literature[17] are considered in approximating the arterial wall thickness because the variation of thickness for mouse aorta with the same age, diet and genotype is small.

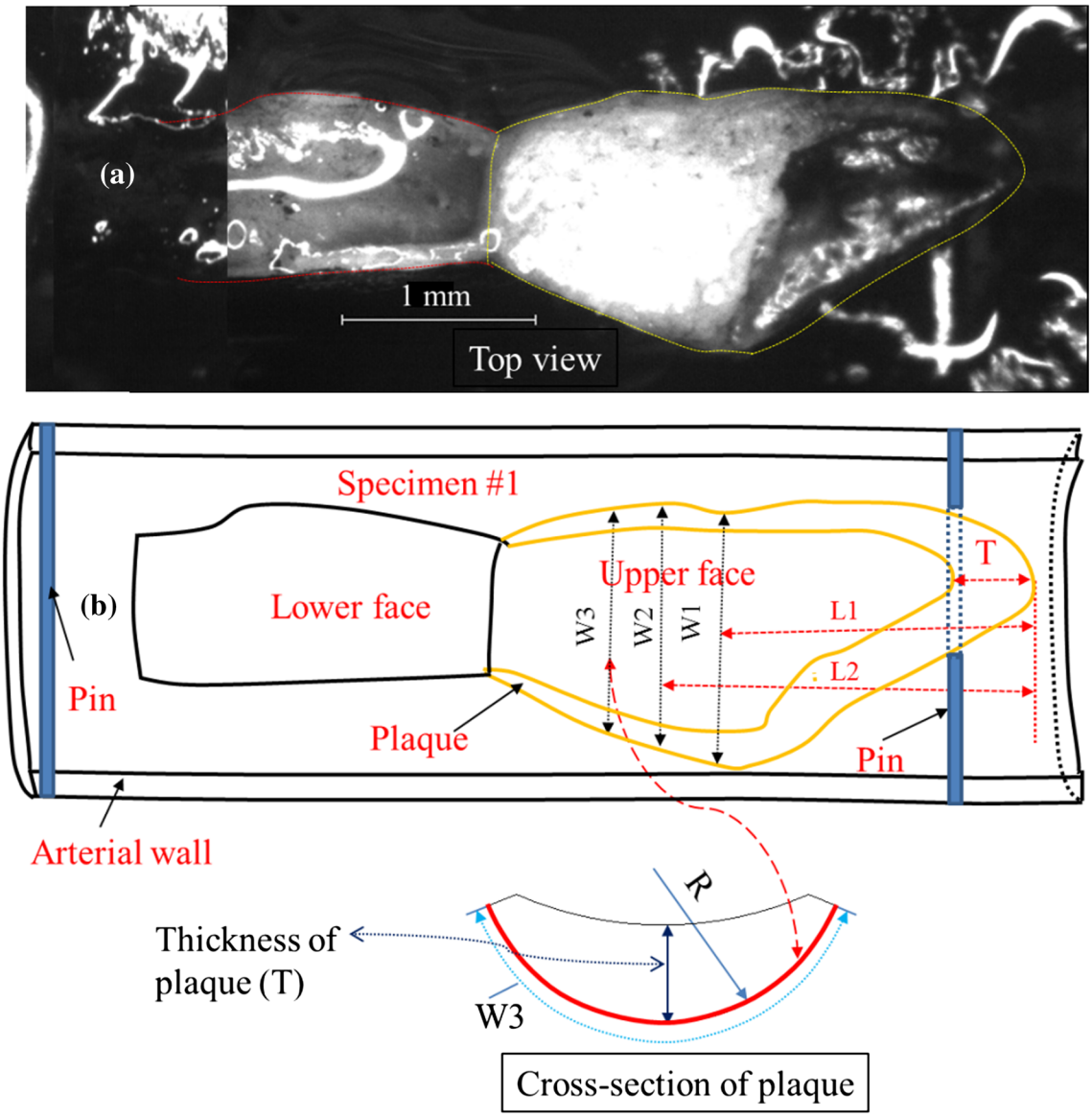

FIGURE 3. (a) An experimental delamination image of a mouse plaque specimen (specimen #1); (b) A schematic of the image in (a) with definitions of the specimen geometry. The "upper face" is the separated surface pulled by the micro-clamp, and the "lower face" is the exposed surface. Scale bar = 1 mm.

Based on these considerations, an approximate geometry model of the plaque specimen is created. The effects of the uncertainties in the geometric values will be examined in "Analysis of the Effects of Geometric Uncertainty" section.

Two Considerations to Define Geometry of Finite Element Model

Delamination Experimental Images

The width and length of the delamination area can be measured directly from the available experimental images. For example, one experimental image of specimen #1 is shown in Fig. 3. Considering the curvature of the lower face, the geometrical values for the plaque are measured from the upper face, in which W1, W2 and W3 are three values of the width used to approximate the cross-section of the mouse atherosclerotic plaque specimen, and L1 and L2 are the distances from the proximal end of the specimen to the positions where W1 and W2 are measured, respectively. The total length of the plaque specimen is determined by the distance from the left pinned end (the proximal end) to the right pinned end (the distal end) of the plaque specimen. The thickness of the plaque, T, can be estimated only at the proximal end from the experimental image. Thus, as an

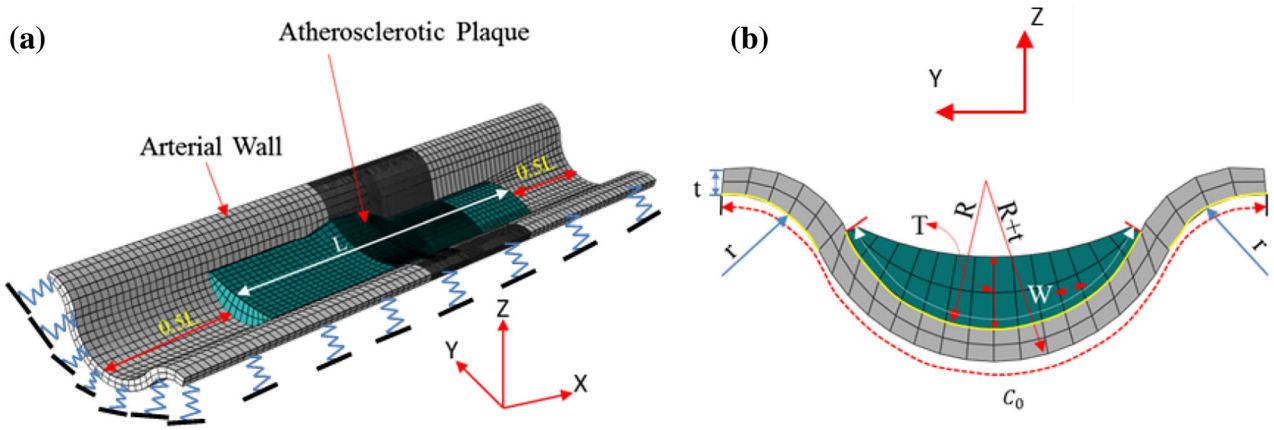

FIGURE 4. A FE model of the mouse aorta (specimen #1): (a) a FE model for delamination simulation, where L is the length of the atherosclerotic plaque; elastic springs under the arterial wall in x, y and z directions represent the underlying connective tissue. (b) a cross-sectional view of the aorta and plaque, showing an idealized geometry described by several parameters, where r is the radius of the aortic wall curvature away from the plaque, *R* is the radius of curvature of the interface between the plaque and the arterial wall, *t* is the thickness of the aortic wall, *W* is the width of the plaque, *T* is the height of the atherosclerotic plaque, and C_o is the total circumferential width of the aortic wall.

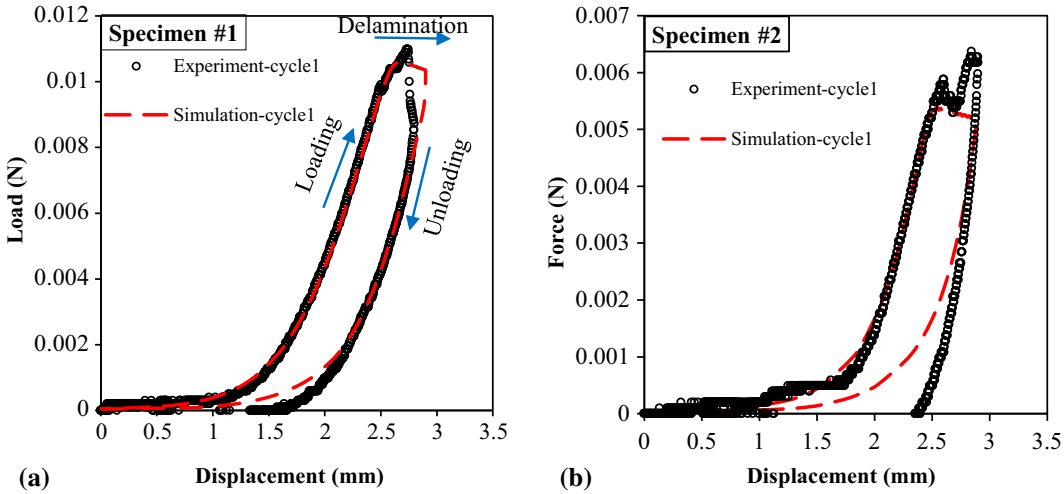

FIGURE 5. (a) The simulated load–displacement curve of the first loading–unloading cycle from specimen #1 is compared with the measured curve, $G_c = 0.019$ *N*/mm. (b) The simulated load–displacement curve of the first loading–unloading cycle from specimen #2 is compared with the measured curve, $G_c = 0.01$ *N*/mm. The entire cycle includes the loading phase in which the plaque is pulled without delamination, the delamination phase in which the plaque is pulled and separated from the underlying internal elastic lamina (IEL), and the unloading phase in which the plaque is returned to the initial position.

approximation, T is taken to be constant along the total length of the specimen in the finite element model. The radius R of the interface between the aortic wall and the plaque is also available only approximately from experimental images.

Geometry Values From the Literature

The literature provides some reference values for the aortic geometry useful in the current study. For example, Ref. 17 studied the remodeling of the zero-stress state of the aorta in apoE-deficient mice at the ages of 10, 28 and 56 weeks, in which aortic rings were excised from several locations along the aorta. The geometry values of the aortic rings at zero-stress state measured from mice at the ages of 28 and 56 weeks from Ref. 17 are employed in the current study to provide a range of approximate geometry values for mice at the age of 43 weeks which were used in the delamination experiments being modeled in the current study. Therefore, for the arterial wall, the range of the inner circumference (C_i) is 1.4–2.8 mm, the range of the outer circumference (C_o) is 2.0–3.3 mm, and the range of the thickness is 0.08–0.16 mm.

TABLE 1. Material parameters of mouse arterial wall and plaque identified from specimen #1.

	μ (kPa)	k_1 (kPa)	k_2	κ	β (°)
Arterial wall	4	4e3	525	0.226	46.4
Plaque	4	4e3	525	0.226	27.2

TABLE 2. Stiffness of springs for specimen #1 and specimen #2.

Specimen	k_x (N/mm^3)	k_y (N/mm^3)	k_z (N/mm^3)
#1	1e−4	1e−4	1e−4
#2	3e−5	5e−5	1e−4

TABLE 3. CZM parameter values.

CZM parameters	T_3^0 (MPa)	T_{shear}^0 (MPa)	K (N/mm^3)	α
Values	0.14	0.14	1e4	1.2

FE Model of the Plaque Delamination Experiments

For the *in situ* experiments, it is difficult to obtain the geometry of the atherosclerotic plaque and the arterial wall, not only because of the complexity of the geometry, but also because of the very small dimensions of the mouse aorta. The geometrical dimensions of the width and length of the atherosclerotic plaque are more accurate because these values can be directly measured from the experimental images, as shown in Fig. 3. In addition, the delaminated area between the plaque and underlying vascular wall shows large variations during the delamination process. Therefore, in building the finite element model, the two contributions in "Two Considerations to Define Geometry of Finite Element Model" section are incorporated into the model based on available information. The resulting 3D finite element model with a reasonable approximation of the actual specimen contains an asymmetrical atherosclerotic plaque as shown in Fig. 4.

In the model, the widths of the plaque are measured at different locations along the longitudinal direction of the arterial wall from the experimental images, as shown in Fig. 3. The thickness of the plaque is taken as a constant value for the delamination length of each loading–delamination–unloading cycle (which is around 0.2 mm).

In the experiments, both ends of the specimen were constrained by pins, but the pins could not completely constrain the movement of the specimen along the longitudinal direction, as if the pinned vessel acted as an elastic foundation in the longitudinal direction. Therefore, in the finite element model, the arterial wall is made longer than the plaque, so that the extra length of the arterial wall can provide the needed freedom to model this elastic foundation effect. For simplicity, the lengths of the arterial wall on either side of the plaque, from the two ends of the plaque to the two ends of the arterial wall, are set to equal half the length of the plaque, as shown in Fig. 4a.

Boundary Conditions

Because perivascular adipose tissue[26,30] and other surrounding connective tissues are in close association with the arterial wall and serve as the vascular bed, they are expected to constrain the movement of the arterial wall. Due to limited information regarding the structure and material properties for those tissues, the effects of the underlying tissues are modeled by an elastic foundation under the aortic wall. To this end, the boundary of the arterial wall is approximated by elastic springs that connect points to the ground in x, y and z directions, as shown in Fig. 4a. The proximal and distal ends of the wall are approximated by fixed boundary conditions.

The equations used to describe the response of the tissues connecting to the arterial wall are $F_x = k_x u_x$, $F_y = k_y u_y$ and $F_z = k_z u_z$. The parameters k_x, k_y, k_z are the stiffness values, u_x, u_y, u_z are the displacements, and F_x, F_y, F_z are the spring forces in the three directions, respectively.

Reasonable values of the spring stiffness are chosen as part of a numerical identification procedure that matches simulation predictions of the overall load vs. load-point displacement curve with experimental measurements. In selecting the spring stiffness values, only the loading phase of the load vs. load-point displacement curve is used.

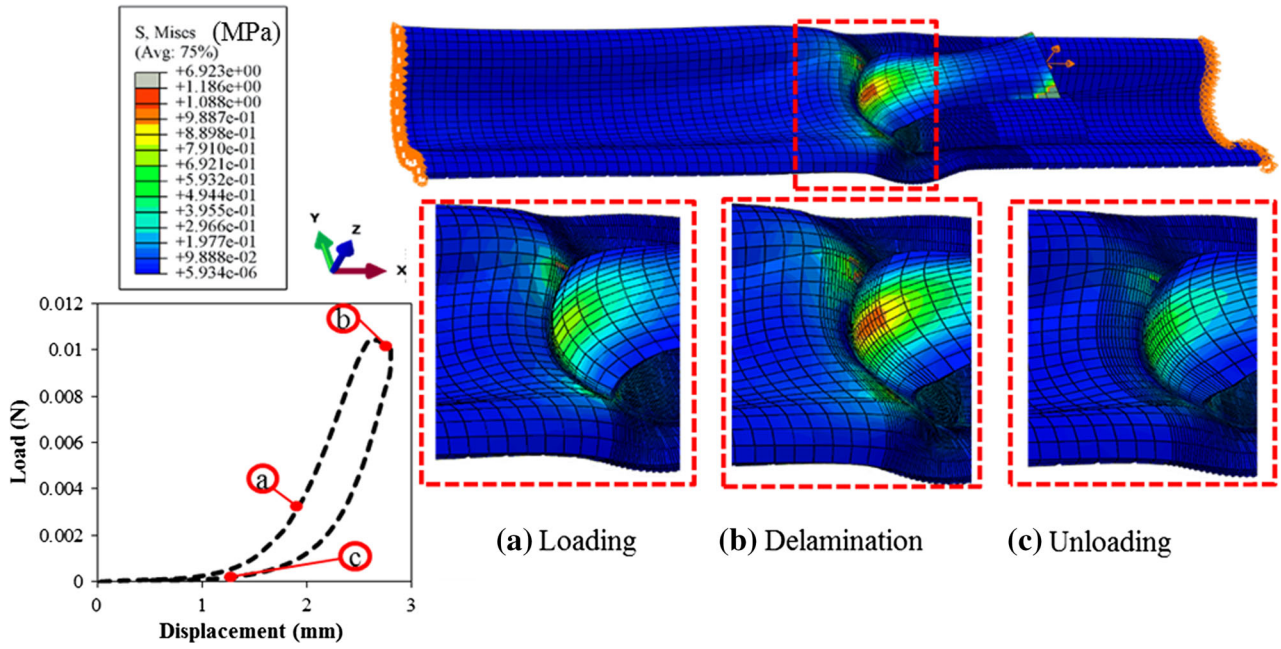

FIGURE 6. von Mises stress contours for three typical points of loading–unloading cycle of plaque delamination simulation from specimen #1.

Figure 4 shows a complete finite element model using the geometry described earlier. The mesh is generated using ABAQUS.[2] The arterial wall and plaque regions are meshed with 8-node brick elements, C3D8H, while the cohesive zone interface is meshed with zero thickness 8-node 3D user-defined elements. A layer of cohesive elements is placed along the delamination path, starting from the initial crack front to the end of the plaque. It is noted that while the CZM approach can handle material separation without a given separation path, it will greatly save the computational cost if the separation path is not part of the simulation prediction. In the current study, since the material separation path in the experiments being simulated is known in advance, the delamination path is taken as known in order to save computational effort and to avoid complexities associated with the need to predict the separation path. The global bulk element size (for the arterial wall and plaque) is 0.1 mm and the cohesive element size is 0.02 mm.

Parameter Value Identification

The parameter values for the bulk arterial material, the elastic springs, and the CZM, are obtained through an inverse identification procedure that matches simulation predictions of the overall load vs. load-point displacement curve with experimental measurements. Since the current study involves many parameters, and only a limited amount of experimental data are available, a fully automated inverse procedure[7] will be very time consuming and thus was not employed. Instead, approximations were made (e.g., most of the bulk material parameter values were set to be the same for the arterial wall and for the plaque), simple values were chosen (e.g., single-digit rounded values were chosen for the elastic foundation spring constants), and a manual numerical procedure[6] was performed. The experimental load vs. load-point displacement curve for the first loading–delamination–unloading cycle from specimen #1 and reference parameter values from the literature are used as the input data for the identification procedure. In this study, a set of parameter values is determined when the average error, $e_{\text{avg}} = \left[\sum_{i=1}^{N}\left(\frac{f_{\text{sim}}-f_{\text{exp}}}{f_{\text{exp}}}\right)\right]/N$, between simulation predicted reaction forces, f_{sim}, and experimentally measured reaction forces, f_{exp}, is less than 10%, where N is the number of data points which spread over the loading, delamination and unloading phases of the load–displacement curve for the first loading cycle. A relatively large error (10%) is accepted because the match between simulation predictions and experimental data is expected not to be perfect due to several uncertainties in the simulation model and input data.

Parameter Values for the HGO Model and Elastic Springs

Reference 29 investigated the stress strain response of aortas from ApoE$^{-/-}$Fbn1$^{+/C1039G}$ and ApoE$^{-/-}$ mice that were fed with normal chow or Western-style (high-fat) diets for 10 and 20 weeks. It was observed

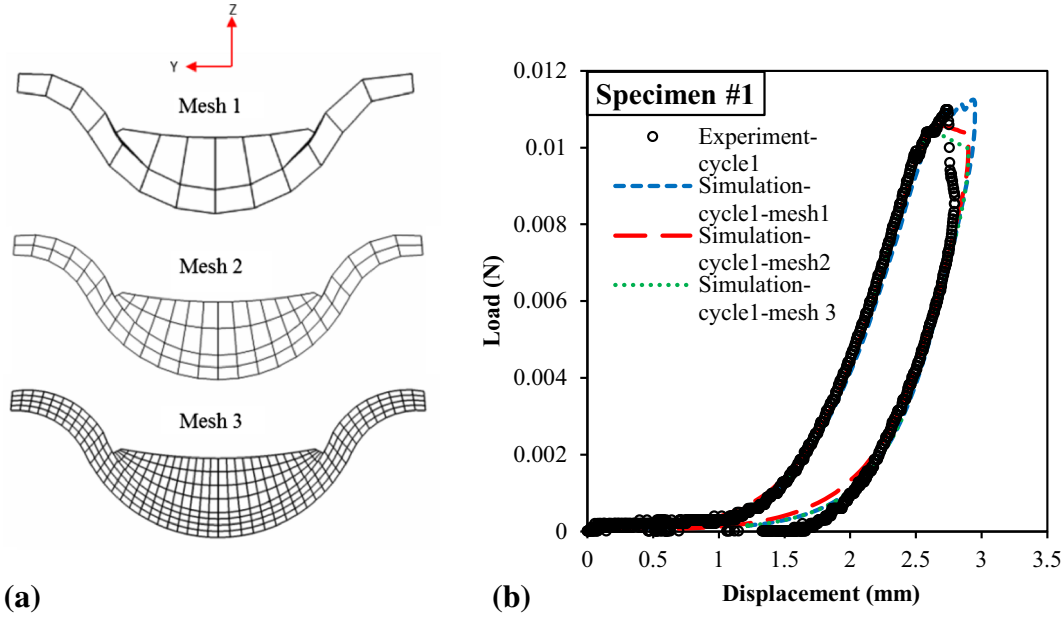

FIGURE 7. (a) Cross-section of three different meshes, (b) predicted 1st-cycle load–displacement curves using the three meshes, with comparison to the experimental curve.

that the stiffness of the mouse aorta not only increases with age but also correlates with the diet. For the experiments being modeled in the current paper, the mice were fed a Western-style diet for 34 weeks, which means that the stiffness of the mouse aorta is expected to be greater than those reported in Ref. 29 Similarly, the values of the HGO model parameters reported in the literature for mouse aorta refer to mice at the age near 10 weeks,[8,9,11] which means that they are not directly applicable in the current study.

Therefore, the values for HGO model parameters for the bulk material and the values of the stiffness of elastic springs are determined based on values suggested in the literature[8] and by matching simulation predictions with measurements using the loading phase of the load–displacement curve from the 1st loading–unloading cycle of specimen #1 ($e_{\text{avg}} = 6.37\,\%, N = 54$), as shown in Fig. 5a. In carrying out this identification procedure, the deformations of arterial wall and plaque are also checked to make sure that they are consistent with those observed experimentally.

The arterial wall and plaque are treated as two layers of heterogeneous materials. As a first-order approximation, their HGO model parameter values are chosen mostly to be the same, due to the lack of proper literature reference data and the lack of sufficient experimental data for more adequate inverse identification. These HGO model parameter values are shown in Table 1. The values of the stiffness of elastic springs in the elastic foundation under the arterial wall are listed in Table 2. Meanwhile, with the same HGO model parameter values (Table 1) identified from specimen #1, the values of the elastic springs for specimen #2 (Table 2) were obtained through matching simulation predictions with measurements using the loading phase of the load–displacement curve from the 1st loading–delamination–unloading cycle of specimen #2, as shown in Fig. 5b. The stiffness values are smaller than those for human and porcine adipose tissues (which have elastic moduli of approximately 1 kPa).[1,10]

The simulation predicted von Mises stress contours for three typical points along a loading–delamination–unloading cycle from specimen #1 are shown in Fig. 6. The stress contour levels shown in the zoomed-in views (a), (b) and (c) are consistent with the corresponding loading levels in the load–displacement diagram. For example, the loading level in (b) is the highest and is sufficient to grow the delamination, and the resulting von Mises stress field shows that it has the highest contour level of the three cases. In all three cases, the highest stress contour level occurs in the middle portion of the plaque near the delamination front, which is expected. In (b), the highest stress level is located somewhat behind the delamination front, which is consistent with the fact that the loading level in (b) occurs somewhat after the peak load is reached in the load–displacement diagram.

CZM Material Properties

In the current study, the delamination of atherosclerotic plaque is approximated as a pure Mode I process,[32] in which the dominant cohesive traction is the tensile cohesive traction normal to the plane of

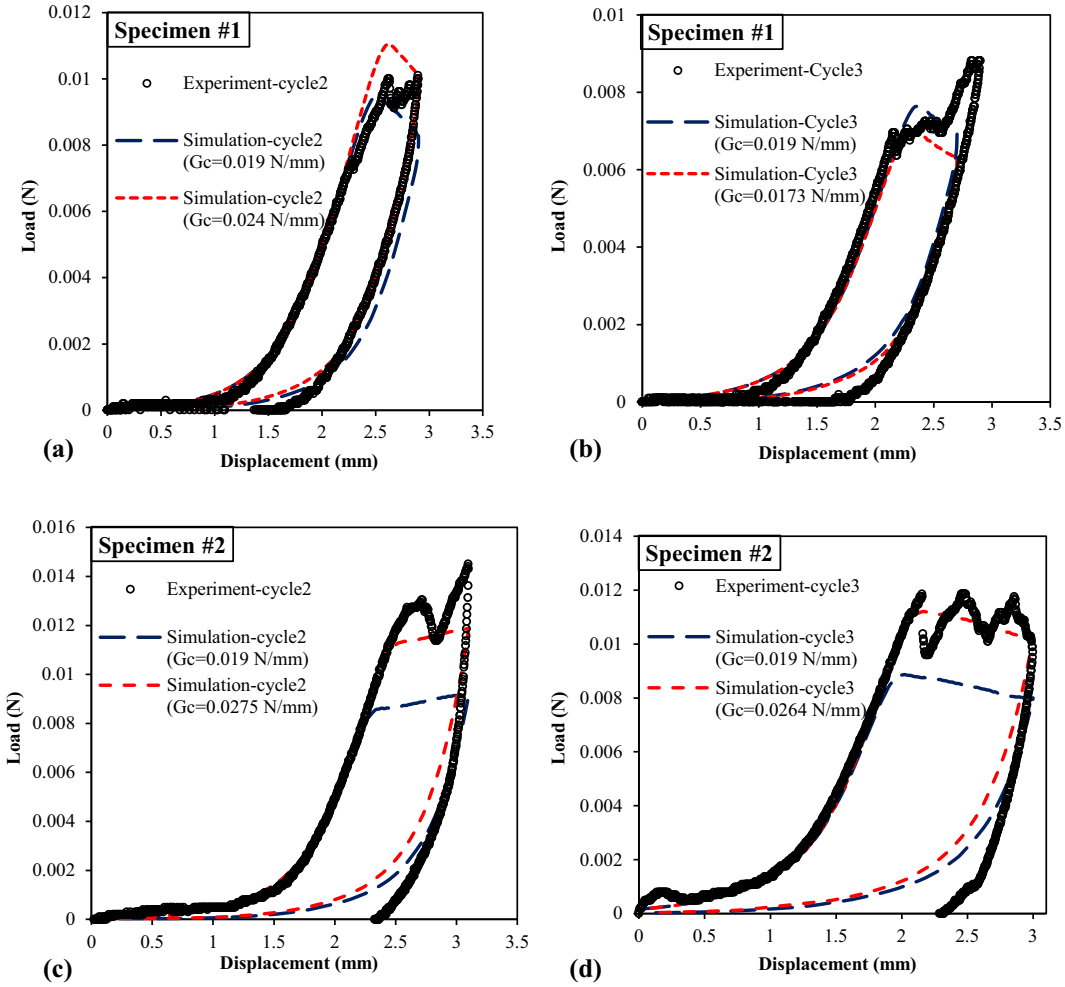

FIGURE 8. Comparisons of the predicted and measured load–displacement curves for loading–unloading cycles. (a) cycle 2 and (b) cycle 3 of specimen #1; (c) cycle 2 and (d) cycle 3 of specimen #2.

delamination. Therefore, for simplicity, the values of G_{IIc} for all cycles are set to be equal to G_{Ic}, because the exact value of this Mode II parameter in a Mode I event has negligible effect on the simulation results. Due to the variation in geometry of the delamination area and material heterogeneities along the longitudinal direction of the aorta, the energy release rate in pure Mode I, G_{Ic}, varied from one delamination cycle to another.[32] The measured G_{Ic} values are used as the input cohesive parameter values.

The rest of the CZM parameter values, as shown in Table 3, are selected based on values suggested in the literature, such as the tensile strength of the interface between the plaque and the underlying tissue (the arterial wall),[14] and by matching simulation predictions of the load–displacement curve with measurements using the delamination phase of the first loading–delamination–unloading cycle of specimen #1 (as shown in Fig. 5a). Care was taken to ensure that the deformations of the arterial wall and the plaque during the delamination phase are consistent with those from experimental measurements, as described earlier for determining parameter values of the HGO model for the bulk arterial wall and plaque behavior.

Convergence Analysis

A convergence study was performed on the bulk material element and the cohesive element in order to exclude mesh dependency effects. Mesh 1 is a coarse mesh with 3472 nodes and 1972 brick elements (C3D8H), mesh 2 (the reference mesh) is refined from Mesh 1 (the element size in Mesh 2 is half of that in Mesh 1, along x, y and z directions) with 19,446 nodes and 14,136 brick elements, and mesh 3 is refined from mesh 2 with 119,365 nodes and 99,423 brick elements (the cross-sections of three meshes are shown in Fig. 7a).

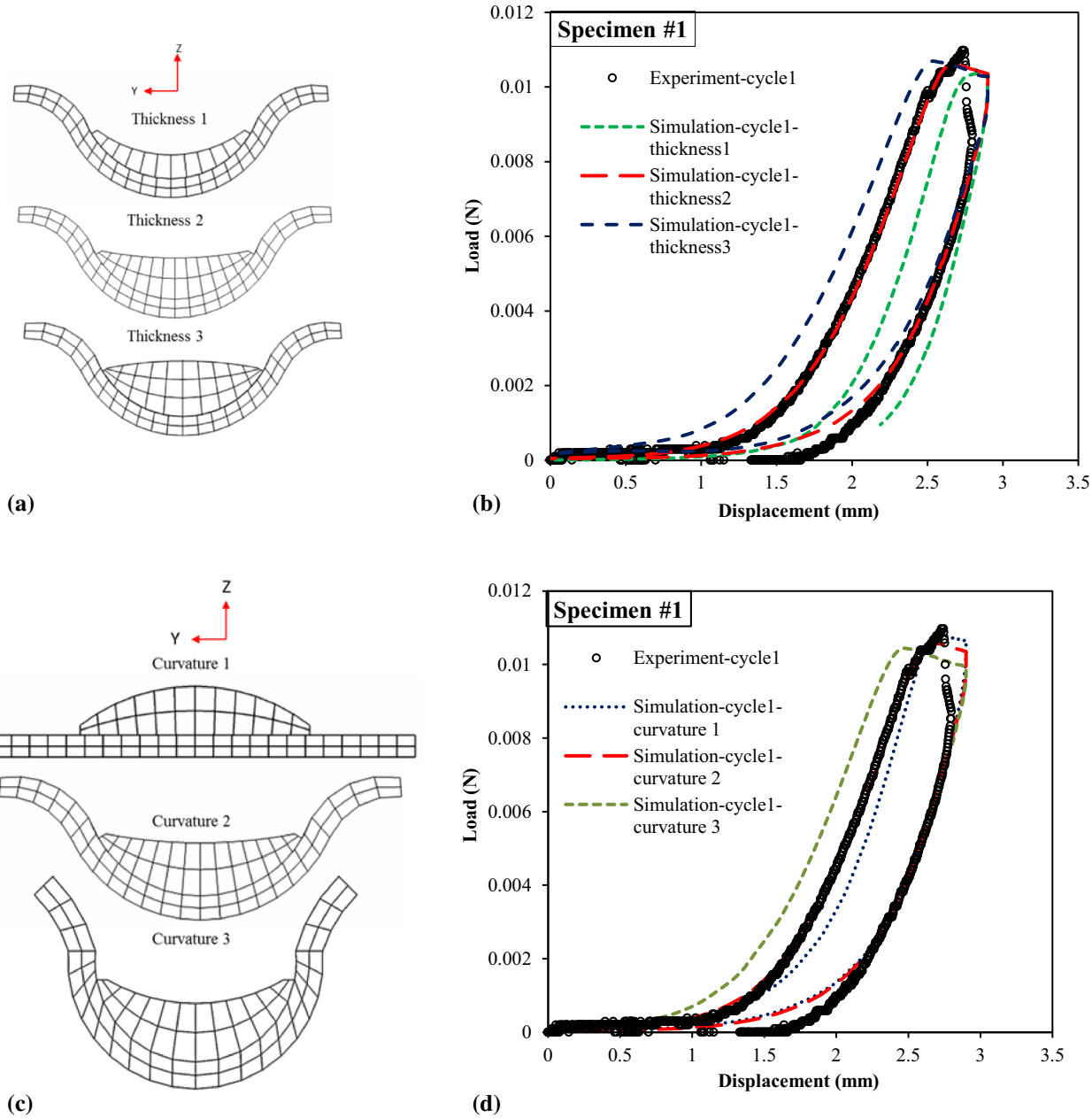

FIGURE 9. Analysis of the effects of the geometric uncertainty: (a) The cross-sections of finite element models with three typical atherosclerotic plaque thicknesses. (b) Predicted load–displacement curves from simulations with three different thicknesses. (c) The cross-sections of finite element models with three typical atherosclerotic plaque curvatures. (d) Predicted load–displacement curves from simulations with three different curvatures.

The cohesive element size is dictated by the bulk material element size along the delamination path. Specifically, the cohesive element size, l_e, is 0.04, 0.02, 0.01 mm, respectively, for the three different meshes. It is observed that, from one mesh to another, there is little change in the predicted loading and unloading phases of the load–displacement curve, as shown in Fig. 7b. The average value of the pulling load during the delamination phase is constant and defines a plateau, which decreases with the decrease of the element size. The average relative errors for mesh 1 and mesh 3 compared to mesh 2 are 3.6 and 2.3%, respectively. Overall, mesh 2 is found to give reasonably converged predictions.

PREDICTION AND VALIDATION

Simulation predictions and validation of the predictions are performed for loading–delamination–unloading cycles 2 and 3 from both specimen #1 and specimen #2, using the HGO model and CZM parameter values determined according to the parameter identification procedure, based on the 1st loading–delamination–unloading cycle of the experimental load–displacement curve for specimen #1. The stiffness values of the elastic foundation springs for the two specimens are determined, respectively, from cycle 1 of each specimen, and are listed in Table 2.

Two simulations for each cycle are carried out due to two input choices for each cycle. Specifically, for each cycle, there are two choices for the critical energy release rate input value: (1) the experimental value from the corresponding cycle (see the red short dashed line in Fig. 8), and (2) the value is kept the same as in cycle 1 of specimen #1 (see the blue long dashed line in Fig. 8). The first choice is more reasonable because it reflects the variation of the experimental critical energy release rate value from cycle to cycle. Simulations with the second choice are made for comparison purposes.

It can be seen from Fig. 8 that the simulation predictions using the critical energy release rate from the corresponding loading cycles provide better predicted average values for the load during the delamination phase of the loading cycle. There are some differences between the predictions and measurements, especially for the delamination and unloading phases. There are several possible reasons for these differences. In the experiments, the tissue along the delamination path may not be homogeneous. It may contain weak material (e.g., lipid cores) and strong material (e.g., bridging fibers and calcification in the tissue), which can lead to oscillations in the delamination load. In the simulations, however, material inhomogeneity is not taken into consideration, thus oscillations in the delamination load are not predicted. The larger difference in the unloading curve is believed to be caused by the fact that the HGO model is not capable of modeling the viscoelastic behavior in the bulk material, while in the delamination experiments the viscoelastic effect may be non-negligible. Moreover, the differences may be caused by the approximations and simplifying assumptions made in the simulation models due to the lack of experimental data for geometrical dimensions and material model parameters, and by the choices of the material models themselves. Overall, the simulation predictions match reasonably well with the experimental measurements. Thus, it can be said that a good validation for the CZM-based simulation approach for the plaque delamination process has been achieved, although further improvements in the overall simulation model are still necessary.

ANALYSIS OF THE EFFECTS OF GEOMETRIC UNCERTAINTY

There are several uncertainties in the simulation model for the plaque delamination experiments, which may partly be responsible for the differences observed in the comparisons between simulation predictions and experimental results shown in Fig. 8. Besides uncertainties in the material parameter values, a key uncertainty is in the geometry of the mouse aorta. The effects of this uncertainty are analyzed in this section and specimen #1 is chosen for this purpose.

In the simulations, the thickness of the plaque and curvature of the arterial wall are taken to be constant along the length of the aorta due to the lack of experimental data. In reality, the thickness of the plaque and curvature of the arterial wall vary along the longitudinal direction of the aorta. To gain some insight into the effect of plaque thickness on simulation predictions, three plaque thickness values are considered: 0.15 mm (thickness-1), 0.26 mm (thickness-2) and 0.35 mm (thickness-3) (Fig. 9a). Furthermore, to study the effect of the aortic curvature in the cross-section on simulation predictions, three shapes of the cross-section are considered based on the curvature of the aorta below the plaque: 0.00 mm^{-1} (curvature-1), 1.69 mm^{-1} (curvature-2), and 2.22 mm^{-1} (curvature-3) (Fig. 9c). All other aspects of the simulation model stay the same.

The simulation predicted load–displacement curves are shown in Fig. 9 along with experimental data. It is seen that the predicted maximum load is only slightly affected by the plaque thickness, as shown in Fig. 9b. However, the loading and unloading phases (especially the loading phase) of the load–displacement curve are strongly affected by the plaque thickness. The reason for these observed thickness effects seems to be related to the fact that when the thickness is changed, the structural stiffness of the model is changed (but not the delamination resistance of the interface), which is why the loading/unloading response is strongly affected (but not the peak load, which is more dictated by the delamination resistance).

In addition, the unloading phase of the load–displacement curve is not much affected by the curvature, but the loading and delamination phases of the load–displacement curve are more strongly affected by the curvature, as shown in Fig. 9d. A straightforward explanation for the predicted effects of the curvature is not clear at this time. This is because, when the curvature changes, several possibly coupled effects may be

involved, including differences in the reactions of the foundation springs, the effects on the overall structural stiffness, and the effects on the energy release rate.

CONCLUSIONS AND CLOSING REMARKS

Plaque delamination often occurs at the shoulder region of the fibrous cap. Studies of atherosclerotic plaque delamination in mouse specimens provide a way to understand the mechanisms of arterial failure and damage evolution at material layer interfaces. There are studies that focus on the analysis of stress–strain behavior and tissue dissection inside the arterial material,[13–15] but few studies have investigated the delamination of atherosclerotic plaque from the underlying arterial wall.

In the present work, a finite element based modeling approach for simulating atherosclerotic plaque delamination events has been developed and demonstrated. Simulations of plaque delamination experiments on mouse aorta specimens have been carried out, in which the HGO model for the bulk arterial material behavior and the CZM for the delamination behavior along the plaque-media interface are adopted. The 3D geometry model is generated based on images from the plaque delamination experiments and on geometric values from the literature.

Parameter values for the HGO model and the CZM were determined based on values suggested in the literature, by matching simulation predictions of the first loading–delamination–unloading cycle of the load–displacement curve from specimen #1 with the measured curve, and by requiring that the predicted deformations be consistent with those from experimental measurements. As validation of the CZM approach, the parameter values identified from the first loading–delamination–unloading cycle of specimen #1 were employed for one group of simulations for loading cycles 2, 3 from specimen #1 and another group of simulations for loading–unloading cycles 2, 3 from specimen #2. The simulation predictions of the load–displacement curves for these cycles were found to match reasonably well with experimental curves.

Furthermore, the simulation model was used to study the effects of geometric uncertainty on simulation predictions. It was found that the predicted load in the delamination phase was not affected by the plaque thickness, but it was strongly affected by the curvature of the arterial wall in cross-section.

While the geometric uncertainty and associated simplifications and approximations for the simulation model may be partly responsible for the differences seen in the comparisons between simulation predictions and experimental results, approximations in modeling the bulk material behavior for the arterial wall and for the plaque are also expected to contribute to the observed differences. First, it is known that the mechanical behavior of the plaque is in general different from that of the arterial wall. In the current study, the plaque was modeled using the HGO constitutive model which was developed for the arterial wall. The HGO model may not be appropriate for the plaque because the histological components of the plaque are different from those of the arterial wall.[21] Hence, a more suitable constitutive model for the plaque is needed. Second, due to the lack of experimental data, several of the HGO model parameter values for the arterial wall and for the plaque were simply chosen to be the same in the current study, which may be grossly inadequate. Third, adventitia, media and intima are three layers in the arterial wall which in general have different material properties, but they are lumped together in the current study as a single layer. Fourth, experimental data show the existence of hysteresis behavior in the load–displacement curve, which suggests that there may be a need to consider the viscoelastic behavior of the arterial wall and the plaque.

ACKNOWLEDGMENTS

Research reported in this publication was supported by the National Science Foundation (NSF) under Awards Number CMMI-1200358. The authors thank Ms Lindsey Davis for her assistance with the use of experimental data.

CONFLICT OF INTEREST

No benefits in any form have been or will be received from a commercial party related directly or indirectly to the subject of this manuscript.

REFERENCES

[1]Alkhouli, N., J. Mansfield, E. Green, J. Bell, B. Knight, N. Liversedge, J. C. Tham, R. Welbourn, A. C. Shore, K. Kos, and C. P. Winlove. The mechanical properties of human adipose tissues and their relationships to the structure and composition of the extracellular matrix. *Am. J. Physiol. Endocrinol. Metab.* 305:E1427–E1435, 2013.

[2]ABAQUS, Analysis User's Manual Version 6.12. Dassault Systemes Corp, 2013.

[3]Badel, P., S. Avril, M. A. Sutton, and S. M. Lessner. Numerical simulation of arterial dissection during balloon angioplasty of atherosclerotic coronary arteries. *J. Biomech.* 47(4):878–889, 2014.

[4]Benzeggagh, M. L., and M. Kenane. Measurement of mixed-mode delamination fracture toughness of unidirectional glass/epoxy composites with mixed- mode bending apparatus. *Compos. Sci. Technol.* 49:439–449, 1996.
[5]Camanho, P. P., C. G. Dávila, and M. F. de Moura. Numerical simulation of mixed-mode progressive delamination in composite materials. *J. Compos. Mater.* 37(16):1415–1438, 2003.
[6]Chen, X., X. Deng, and M. A. Sutton. Simulation of stable tearing crack growth events using the cohesive zone model approach. *Eng. Fract. Mech.* 99:223–238, 2013.
[7]Chen, X., X. Deng, M. A. Sutton, and P. Zavattieri. An inverse analysis of cohesive zone model parameter values for ductile crack growth simulations. *Int. J. Mech. Sci.* 79:206–215, 2014.
[8]Collins, M. J., M. Bersi, E. Wilson, and J. D. Humphrey. Mechanical properties of suprarenal and infrarenal abdominal aorta: implications for mouse models of aneurysms. *Med. Eng. Phys.* 33(10):1262–1269, 2011.
[9]Collins, M. J., J. F. Eberth, E. Wilson, and J. D. Humphrey. Acute mechanical effects of elastase on the infrarenal mouse aorta: implications for models of aneurysms. *J Biomech* 45(4):660–665, 2012.
[10]Comley, K. and N. Fleck. The mechanical response of porcine adipose tissue. ASME J. Biomech. Eng. 1–30, 2009.
[11]Eberth, J. F., A. I. Taucer, E. Wilson, and J. D. Humphrey. Mechanics of carotid arteries in a mouse model of Marfan Syndrome. *Ann. Biomed. Eng.* 37(6):1093–1104, 2009.
[12]Ferrante, G., P. Presbitero, R. Whitbourn, and P. Barlis. Current applications of optical coherence tomography for coronary intervention. *Int. J. Cardiol.* 165:7–16, 2013.
[13]Ferrara, A., and A. Pandolfi. A numerical study of arterial media dissection processes. *Int. J. Fract.* 166(1–2):21–33, 2010.
[14]Gasser, T. C., and G. A. Holzapfel. Modeling the propagation of arterial dissection. *Eur. J. Mech. A* 25(4):617–633, 2006.
[15]Gasser, T. C., and G. A. Holzapfel. Modeling plaque fissuring and dissection during balloon angioplasty intervention. *Ann. Biomed. Eng.* 35(5):711–723, 2007.
[16]Gasser, T. C., R. W. Ogden, and G. A. Holzapfel. Hyperelastic modelling of arterial layers with distributed collagen fibre orientations. *J. R. Soc. Interface* 3(6):15–35, 2006.
[17]Gregersen, H., J. Zhao, X. Lu, J. Zhou, and E. Falk. Remodeling of the zero-stress state and residual strains in apoE-deficient mouse aorta. *Biorheology* 44(2):75–89, 2007.
[18]Holzapfel, G. A. Biomechanics of soft tissue. In: Handbook of Materials Behavior Models: Composite Media, Biomaterials1st, edited by J. Lemaitre. Boston: Academic, 2001, pp. 1057–1071.
[19]Holzapfel, G. A., T. C. Gasser, and R. W. Ogden. A new constitutive framework for arterial wall mechanics and a comparative study of material models. *J. Elast.* 61(1):1–48, 2000.
[20]Honye, J., D. J. Mahon, A. Jain, C. J. White, S. R. Ramee, J. B. Wallis, A. al-Zarka, and J. Tobis. M, Morphological effects of coronary balloon angioplasty in vivo assessed by intravascular ultrasound imaging. *Circulation* 85:1012–1025, 1992.
[21]Huang, H., R. Virmani, H. Younis, A. P. Burke, R. D. Kamm, and R. T. Lee. The impact of calcification on the biomechanical stability of atherosclerotic plaques. *Circulation* 103(8):1051–1056, 2001.
[22]Loree, H. M., R. D. Kamm, R. G. Stringfellow, and R. T. Lee. Effects of fibrous cap thickness on peak circumferential stress in model atherosclerotic vessels. *Circ. Res.* 71(4):850–858, 1992.
[23]Meir, K. S., and E. Leitersdorf. Atherosclerosis in the apolipoprotein-E-deficient mouse: a decade of progress. *Arterioscler. Thromb. Vasc. Biol.* 24(6):1006–1014, 2004.
[24]Nakashima, Y., A. S. Plump, E. W. Raines, J. L. Breslow, and R. Ross. ApoE-deficient mice develop lesions of all phases of atherosclerosis throughout the arterial tree. *Arterioscler. Thromb. Vasc. Biol.* 14(1):133–140, 1994.
[25]Sakai, S., K. Mizuno, S. Yokoyama, J. Tanabe, T. Shinada, K. Seimiya, M. Takano, T. Ohba, M. Tomimura, R. Uemura, and T. Imaizumi. Morphologic changes in infarct-related plaque after coronary stent placement: a serial angioscopy study. *J. Am. Coll. Cardiol.* 42(9):1558–1565, 2003.
[26]Szasz, T., G. F. Bomfim, and R. C. Webb. The influence of perivascular adipose tissue on vascular homeostasis. *Vasc. Health Risk Manag.* 9:105–116, 2013.
[27]Tearney, G. J., *et al.* Consensus standards for acquisition, measurement, and reporting of intravascular optical coherence tomography studies: a report From the International Working Group for Intravascular Optical Coherence Tomography Standardization and Validation. *J. Am. Coll. Cardiol.* 59(12):1058–1072, 2012.
[28]Turon, A., P. P. Camanho, J. Costa, and C. G. Dávila. A damage model for the simulation of delamination in advanced composites under variable-mode loading. *Mech. Mater.* 38(11):1072–1089, 2006.
[29]Van Herck, J. L., G. R. De Meyer, W. Martinet, C. E. Van Hove, K. Foubert, M. H. Theunis, S. Apers, H. Bult, C. J. Vrints, and A. G. Herman. Impaired fibrillin-1 function promotes features of plaque instability in apolipoprotein E-deficient mice. *Circulation* 120(24):2478–2487, 2009.
[30]Verhagen, S. N., and F. L. Visseren. Perivascular adipose tissue as a cause of atherosclerosis. *Atherosclerosis* 214(1):3–10, 2011.
[31]Virmani, R., J. Narula, M. B. Leon, and J. T. Willerson (eds.). The Vulnerable Atherosclerotic Plaque: Strategies for Diagnosis and Management. Malden: Blackwell Futura, pp. 37–59, 2007.
[32]Wang, Y., J. Ning, J. A. Johnson, M. A. Sutton, and S. M. Lessner. Development of a quantitative mechanical test of atherosclerotic plaque stability. *J. Biomech.* 44(13):2439–2445, 2011.